Computational Biology and Chemistry 121 (2026) 108859

Contents lists available at ScienceDirect

Computational Biology and Chemistry

journal homepage: www.elsevier.com/locate/cbac

Targeted anticancer potential of oxazole derivative against breast cancer: Synthesis, molecular docking, dynamics simulation, and in vitro evaluation on ERBB3 receptor

Jianxing Xu [a,b], Dongwei Zhu [c], Kanagaraj Rajalakshmi [c], Mangirish Deshpande [d], Natarajan Kiruthiga [e], Panneerselvam Theivendren [f,*], Selvaraj Muthusamy [c,*], Siyi Wu [g,*], Weizhong Zhao [a,b,**]

[a] Department of Radiology, Wujin Hospital Affiliated with Jiangsu University, Changzhou 213002, China
[b] Department of Radiology, The Wujin Clinical college of Xuzhou Medical University, Changzhou 213002, China
[c] Department of Immunology, Jiangsu Key Laboratory of Laboratory Medicine, School of Medicine, School of Chemistry and Chemical Engineering, Jiangsu University, Zhenjiang 212013, PR China
[d] Department of Pharmacology, PES's Rajaram and Tarabai Bandekar College of Pharmacy, Ponda, Goa 403401, India
[e] Department of Pharmaceutical Chemistry, KMCH college of Pharmacy, Kalappatti road, Coimbatore, Tamil Nadu 641048, India
[f] Department of Pharmaceutical Chemistry & Analysis, School of Pharmaceutical Sciences, Vels Institute of Science, Technology & Advanced Studies, Pallavaram, Chennai, Tamilnadu 600117, India
[g] Department of Pathology, The Affiliated Taizhou People's Hospital of Nanjing Medical University, Taizhou, Jiangsu 225300, PR China

ARTICLE INFO

Keywords:
Oxazole derivative
ERBB3 receptor
Breast cancer
Molecular docking
Anticancer activity

ABSTRACT

The study investigates 5- ((2-nitrobenzylidene) amino 2-phenyloxazole-4-carbonitrile (PS13), a derivative of the oxazole that was designed to block the ERBB3 receptor that plays a role in breast cancer development. The syntheses of PS13 were performed in two steps due to condensation and its structure was verified with the help of IR NMR, MS, and elemental analysis. Strong binding affinity was observed between the molecules and ERBB3 with the docking score of −9.5 kcal/mol that was reinforced by the presence of key hydrogen and hydrophobic bonds. Simulation of molecular dynamics above 500 ns showed that the formation of the ligand-receptor complex was stable, and the fluctuations of RMSD were minimal, which proves the structural compatibility of the molecules and the stability of their interaction. The ADMET profiling predicted good drug-like, gastrointestinal absorption, non-P-gp substrate, and good metabolism. The analysis of density functional theory indicated that the HOMO-LUMO energy gap is −2.27 eV, which indicated the stability of the electronics, and the ability to be reactive. The PS13-SLNs that were developed were PS13-loaded solid lipid nanoparticles that had high encapsulation efficiency (81 +/- 2.16 %), and enhanced release profiles in both the acidic and neutral pH conditions. Both in vitro MTT assays of MCF-7 cells and morphological changes depicted the dose-dependent cytotoxicity with 60.27 ± 0.04 μg/mL of IC_{50}, and morphological changes that were consonant to apoptosis. Drug release kinetics indicated a first-order mechanism and Fickian diffusion, suggesting a controlled release profile. All these combined with the high ERBB3 binding affinity, good pharmacokinetics, stable SLN formulation, and in vitro anticancer efficacy of PS13, indicate that PS13 is a promising lead candidate to advance in preclinical development in the treatment of breast cancer.

1. Introduction

Breast cancer is one of the most common cancers that are commonly diagnosed in women and it has been a significant cause of cancer related deaths across the globe. Its prevalence is still seen across the world regardless of screening, diagnosis and treatment intervention and its

* Corresponding authors.
** Corresponding author at: Department of Radiology, Wujin Hospital Affiliated with Jiangsu University, Changzhou 213002, China.
E-mail addresses: panneerselvam.sps@vistas.ac.in (P. Theivendren), rajselva311@ujs.edu.cn (S. Muthusamy), 2930339808@qq.com (S. Wu), zhaoweizhong0596@163.com (W. Zhao).

https://doi.org/10.1016/j.compbiolchem.2025.108859
Received 18 October 2025; Received in revised form 28 November 2025; Accepted 16 December 2025
Available online 23 December 2025

prevalence of over 2.3 million new cases is reported each year. The disease develops due to uncontrolled growth of the epithelial cells of the breast originated either as ductal or lobular tissue and has enormous heterogeneity in regards to biological behaviour, invasiveness and clinical outcome (Cianciosi et al., 2020; Zabaleta et al., 2020). This heterogeneity has led to ongoing activities that seek to address precision medicine, and this is aimed at increasing specificity of treatment and a decrease in systemic toxicity (Patil et al., 2024a, 2024b; Naiknaware et al., 2025)

Recent advances in the field of molecular pathology, targeted therapy and personalised medicine have placed the focus on receptor dysregulation, especially in the epidermal growth factor receptor (EGFR/ERBB) family (Bansode et al., 2023; Gajare et al., 2021). ERBB3 is emerging as a very important oncogenic driver because it has been identified to be involved in tumorigenesis, immune evasion, metastasis, and resistance to the existing therapy of breast cancer. ERBB3 is heterodimerized with either ERBB2 or ERBB4 and it triggers several intracellular cascades, such as PI3K/AKT, MAPK, STAT5, and mTOR, which induce tumour survival and growth. Therefore, selective ERBB3 inhibition is a promising therapeutic approach to the treatment resistance and improved clinical outcomes (Dinesh et al., 2025; Ramesh et al., 2023; Theivendren et al., 2025; Liu et al., 2023).

The use of heterocyclic scaffolds, especially the oxazole derivatives, has taken a centre-stage in the discovery of new anticancer drugs, owing to their diverse pharmacological characteristics. The oxazole ring system demonstrates good biological activity, good binding potential, and good structural modification ability and it warrants its applicability in contemporary medicinal chemistry (Bansode et al., 2019; Yang et al., 2024) A variety of molecules based on oxazole's exhibit cytotoxic action through tubulin Polyplication, mitochondrial apoptosis, DNA fragmentation, or antiangiogenic activities. It is important to note that their capacity to bind receptor targets like the HER2, ERBB3, aromatase makes them more viable in researches concerning breast cancer (Fan et al., 2025; Zhou et al., 2021; Yan et al., 2025; Kunjiappan et al., 2024).

Due to these therapeutic benefits, the current work aims at synthesising and exploring oxazole-4-carbonitriles which is an oxazole analogue that targets ERBB3. The chemical integrity of oxazole-4-carbonitriles was established by the multistep synthesis and IR spectroscopy, NMR, mass spectrometry and elemental analysis. A comprehensive molecular docking study was carried out to establish its therapeutic potential and it was found to have a high binding affinity at the ERBB3 active site. The binding behaviour was also confirmed by molecular dynamics as there was excellent complex stability and few structural changes. Further characterization of the molecules by the frontier molecular orbital analysis showed that the HOMO-LUMO energy gap representing a good balance of reactivity and stability. The prediction software ADMET recommended acceptable physicochemical characteristics, drug-likeness, and gastrointestinal absorption and supported oxazole-4-carbonitriles as a feasible oral drug (Kunjiappan et al., 2024; Sumalatha et al., 2025; Senthamarai Pandi et al., 2025). Again, Solid lipid nanoparticles (SLNs) are emerging as an effective nanocarrier system for breast cancer therapy. SLNs enhances the stability and bioavailability of anticancer drugs while enabling controlled and sustained release at the tumour site. SLNs can be engineered for passive targeting through the enhanced permeation and retention effect and further optimized with surface ligands for active targeting of receptors such as HER2 or folate receptors. These features support improved intracellular drug delivery, reduced systemic toxicity, and overall stronger therapeutic outcomes in breast cancer treatment (Gan et al., 2022; Zhang et al., 2023; Chen et al., 2025; Zhu et al., 2022; Lu et al., 2022). The objective of the study is to synthesize and analyze oxazole-based compound, by using molecular docking, dynamics simulation, in vitro cytotoxicity, and ADMET profiling in order to establish its efficacy in ERBB3-expressing breast cancer cells. This logical thread shows that there is a clear objective in line with the existing gaps in therapy and scientific applicability.

2. Materials and methods

2.1. Target identification

To obtain active molecular components and the relationship among these components with breast cancer-related targets, the research process considered various bioinformatics platforms, such as GeneCards, OMIM, SwissTargetPrediction, g:Profiler, and ShinyGO. Venn diagrams were used to visualise the intersection between these sets of targets. These intersecting circular patterns in the form of diagrams enable the researchers and clinicians to compare easily the shared and exclusive biological factors associated with breast cancer. Venn diagrams help understand how the complexity of diseases can be better by showing similarities and differences between different risk factors. Interestingly, one of the main pathways identified by the findings is the ERBB3 signalling pathway that serves as one of the critical mechanisms used by the malignant cells to escape the immune surveillance. In this mechanism, cancer cells are able to suppress the functions of T-cells, diminishing the immune mechanisms and allowing the development of tumours (Panneerselvam et al., 2022; Mandhadi et al., 2020; Palanichamy et al., 2022).

2.2. Ramachandran plot statistics

Protein Data Bank (PDB) complements their search of experimentally determined structural data of proteins with a database, PDBsum, that gives detailed visual and analytical summaries. PDBsum provides annotated schematic representations, secondary structure diagrams and domain organisation maps, and ligand-binding interaction illustrations, which make users see more of the structural and functional properties of proteins.

The scope of this rich datasets makes them very useful to proteomics researchers, since they facilitate molecular modelling, designing drugs using structures and understanding the mechanism of proteins. Moreover, PDBsum is an open portal to additional analysis software and can be used to study protein architecture more thoroughly. This can be accessed using the following link by the users https://www.ebi.ac.uk/thornton-srv/databases/pdbsum/ (Panneerselvam et al., 2022; Mandhadi et al., 2020; Palanichamy et al., 2022).

2.3. Protein preparation

It is possible to conduct protein preparation through integrated systems like RCSB, PubChem, and CHARMM-GUI that may be used effectively. The step takes place with accessing the three-dimensional structure of the target protein at the RCSB Protein Data Bank (https://www.rcsb.org).

Then, the structures of the ligands are available in.sdf format obtained in PubChem (https://pubchem.ncbi.nlm.nih.gov). The files are subsequently automated into CHARMM-GUI which is a web-based interface that is meant to simplify the process of setting up molecular dynamic's simulation. In CHARMM-GUI, the protein structure is optimised through conformation, removal of crystallographic water molecules and addition of any missed atoms. When the preparation is final the end result (a completed system) can be exported to allow further molecular dynamics research to be conducted to enable a detailed study of protein-ligand interactions and associated biological processes (Panneerselvam et al., 2022; Mandhadi et al., 2020; Palanichamy et al., 2022).

2.4. Docking protocol

AutoDock Vina POAP requires the previously described steps for converting Protein (7PCD) and Ligand (PS13) into PDBQT format. The binding site of ligand to receptor surface appears after establishing a grid box which uses coordinates of $x = 10.06$ and $y = 8.73$ and $z = 13.7$. After

defining the binding site by grid setup, it is time to customize docking parameters. The docking simulation produced by Vina generates the top-ranking stable ligand position as docking output which can enhance analysis of molecular interactions and optimize ligand design (Murugesan, 2022; Patagar et al., 2023).

2.5. Molecular dynamics

The initial protocol for Desmond simulations through Maestro requires users to load their protein structure followed by Protein Preparation Wizard preparation steps. You must start by adding a solvent model along with ions before defining the simulation box measurements. Users can set simulation parameters including temperature, pressure and time step through the Desmond module interface. After finishing setup you can execute the simulation to generate visualization of results which contain trajectory alongside energy data for analyzing molecular dynamics (Murugesan, 2022).

2.6. ADMET studies

Lipophilicity and solubility calculation through SwissADME (http://www.Swiss-ADME.ch/index.php) allows users to evaluate ADME properties. The SmartCyp online platform (https://smartcyp.sund.ku.dk/mol_to_som) uses reactivity evaluation to forecast cytochrome P450-mediated sites of metabolism in molecules. The machine learning prediction system CardioTox found on https://biosig.lab.uq.edu.au/cardiotoxcsm/prediction helps researchers determine drug candidate safety through cardiotoxicity assessment. Take advantage of these digital tools to submit molecular structures which will subsequently produce predictive evaluations or visual results for drug development initiatives (Murugesan, 2022).

2.7. Density functionality theory

The chemical component PS13 was initially obtained in the publicly available PubChem database in.sdf format. These structure files were subsequently loaded into the Spartan'14 graphical interface to minimise the energy in order to get an optimised molecular structure. Then, the calculations of the HOMO and LUMO orbitals of the energy values of the Hartree energy were performed using GaussView 6.0.16. In order to assess the electronic characteristics of PS13, the Hartree energies have been transformed into electron volts (eV), which allows determining the HOMO-LUMO energy gap correctly. This energy gap is a vital measure of the stability of the molecules and the results give an understanding of the general reactivity and the possibility of the PS13 functioning in any biological or chemical system (Murugesan, 2022).

2.8. Synthesis

2.8.1. Step 1

A mixture of 0.67 g of benzoyl chloride (4.8 mmol), 0.32 g amino malononitrile (4.0 mmol) and 0.68 g p-toluenesulfonate (4 mmol) was stirred at room temperature for 20 min, followed by heating at 80°C for 105 min. After completion, the reaction mixture was allowed to cool, and 100 mL of brine was added to dilute the solution. The mixture was then neutralized to pH 8, resulting in the formation of a white precipitate. The precipitate was collected and purified by recrystallization using CH_2Cl_2, yielding 5-(benzylideneamino)-2-phenyloxazole-4-carbonitrile (compound I) with an excellent 90 % yield.

2.8.2. Step 2

0.479 g of Compound 1I (2 mmol) was dissolved in 8.5 mL of 96 % ethanol, after which an 0.304 g of equimolar quantity of 2-nitrobenzaldehyde was added in a single portion using a micropipette. The reaction mixture was refluxed with continuous stirring at 110 °C for 115 min and then allowed to cool naturally to room temperature. A solid product gradually formed and was collected by filtration. The precipitate was washed several times with 5 mL of cold 96 % ethanol to remove impurities. Subsequent recrystallization from boiling ethanol followed by drying afforded the final compound, PS13, in an excellent yield of 82 %. This procedure yielded a purified product suitable for further characterization and biological evaluation.

2.9. Formulation of PS13-encapsulated SLNs (PS13-SLNs)

The production of PS13-encapsulated SLNs happened through an oil-in-water microemulsion procedure which involved high-speed homogenization and ultrasonication steps. Cetyl palmitate (2 g) reached a molten state by dissolving in 5 mL ethanol before being mixed with 5 mg PS13 under one to two minutes of sonication. The mixture of lipids received homogenization with an aqueous surfactant solution comprising 1 % polysorbate-80 and 0.5 % sodium deoxycholate for two hours. In the next step, microemulsion underwent ultracentrifugation using 10,000 revolution per minute for 30 min before a second sonication procedure was performed at 10,000 rpm during 10 min. Freeze-drying of the final suspension lasted 48 h at −80 °C until storage at −20 °C for additional analysis.

2.10. Entrapment evolves and drug load capacity of PS13-encapsulated SLNs

The evaluation of PS13 entrapped in SLNs involved immersing 5 mg SLN samples in 10 mL methanol, followed by centrifugation at 10,000 rpm for 30 min. The amount of PS13 in the supernatant was measured. Entrapped drug efficiency and drug loading capacity were calculated using the following equations:

(1) %EE = [(Total PS13 − Free PS13) / Total PS13] × 100 (2) %DLC = [(Total PS13 − Free PS13) / SLNs weight] × 100

2.10.1. In vitro drug release of PS13-encapsulated SLNs

PS13 release from SLNs was determined using an in vitro dialysis bag diffusion method. 10 mg of SLNs in 5 mL buffer solution were placed in a 3500 Da membrane and immersed in 100 mL acetate buffer (pH 5.5) or phosphate buffer (pH 7.4). The system was shaken at 100 rpm at room temperature to monitor PS13 release. As PS13 diffused, the outer buffer solution was replaced with fresh medium. Samples were separated using 14,000 g centrifugal force at 25°C before PS13 quantification by HPLC analysis.

2.11. Drug release kinetics of PS13-encapsulated SLNs

The kinetic analysis of PS13 release from SLNs was performed by fitting the data to five different models: zero-order, first-order, Higuchi, Korsmeyer-Peppas, and Hixson-Crowell. The drug release behavior of SLNs showed different kinetic patterns depending on the model assumptions.

2.12. Stability studies of PS13-encapsulated SLNs

The chemical stability of PS13-encapsulated SLNs was assessed using 10 % NaCl, 0.5 % BSA, acetate buffers (pH 3.5, 5.5), phosphate buffers (pH 7.2, 9.0), and simulated gastric juice, with three replicates. A 100 μL SLN sample was mixed with 0.5 mL of each medium, vortexed, and incubated at 37 ± 2°C. The λmax value was recorded at specific intervals using UV–visible spectrophotometry to evaluate stability.

2.13. Analysis of PS13-encapsulated SLNs

2.13.1. LC-MS analysis of PS13-encapsulated SLNs

The analysis of PS13-encapsulated SLNs was conducted using a Shimadzu LC-MS system with water and methanol as the mobile phase. The mass spectrometry results, combined with dual separation conditions, enabled precise identification of bioactive compounds based on retention time and mass spectral analysis, confirming the successful delivery and stability of the compounds.

2.13.2. FE-SEM analysis of PS13-encapsulated SLNs

FE-SEM analysis served to evaluate the morphology of SLNs containing PS13 during the study. A quantity of 2 mg freeze-dried material was dispersed in 1 mL of distilled water followed by placement of 2 μL on a glass surface that underwent drying for examination.

2.13.3. FTIR analysis of PS13-encapsulated SLNs

PS13 interactions within SLN formulations were evaluated using a Shimadzu IR Tracer-100 FTIR instrument, with data collected at a resolution of 4 cm^{-1} across the 400–4000 cm^{-1} range. The crystalline structure was assessed by XRD (BRUKER D8 Advance ECO) using Cu $K\alpha_1$ radiation ($\lambda = 1.54060$ Å, 20 keV/30 mA). The Zetasizer Nano ZS 3600 measured the size, PDI, and zeta potential. Morphological features were analyzed via FE-SEM (JEOL JSM6700) after preparing 2 mg of SLN dispersions in water and gold-coating for imaging. The results demonstrated promising drug encapsulation efficiency, long-term stability, and suitable characteristics for pharmaceutical applications.

2.14. In vitro anti-breast cancer activity

MCF-7 cells (NCCS) were cultured in DMEM with 10 % FBS, 100 IU/mL penicillin, and 100 μg/mL streptomycin at 37°C in a 5 % CO_2 atmosphere to reach confluency. Cells were trypsinized, and 1×10^4 cells per well were seeded in 100 μL medium. After 24 h, the medium was removed, and cells were washed. Test compounds (100 μL) were added, and cells were incubated for another 24 h. Following the removal of the test solution, 20 μL of MTT solution (2 mg/mL in PBS) was added. After incubation, 100 μL DMSO was added to dissolve formazan, and absorbance was measured at 570 nm. Cell viability was calculated by dividing the sample absorbance by the control absorbance and multiplying by 100. Cell line MCF-7 acquired from NCCS was cultured in DMEM nutrient media containing 10 % FBS and penicillin at 100 IU/mL and streptomycin at 100 μg/mL in an environment of 5 % CO_2 at 37°C with humidity until cells reached full coverage in a culture vessel. The process of trypsinization produced a cell density of 1.0×105 cells/mL which was then distributed into 100 μL volumes in each 96-well plate. Cells received test concentrations of samples followed by longer incubation before getting examined via MTT analysis. Cell viability was evaluated through the microplate reader analysis of 570 nm absorbance.

3. Results and discussion

3.1. Target identification

This work investigated PS13 compound targets in breast cancer by evaluating its interaction with the ERBB3 signaling pathway as well as proteins within its network. The first bar chart demonstrated the target involvement numbers where breast cancer revealed 10,242 known targets but PS13 showed 102 molecular targets along with 57 targets that overlapped between both datasets. The substantial number of shared targets indicates that the compound has significant therapeutic implications for breast cancer treatment Fig. 1.

3.2. Network pharmacology

The field of network pharmacology is important in the realisation of the complexity of the drug action, particularly in a disease such as cancer that is a multifaceted disease that is associated with intricate interactions of molecules. Network pharmacology in the present study was used to examine the biological pathways and the molecular targets of PS13 which is an oxazole analogue against ERBB3 in breast cancer. Conventional drug discovery is usually based on a single molecular target whereas cancer is caused by the dysregulation of several interacting signalling pathways. Network pharmacology can be more holistic

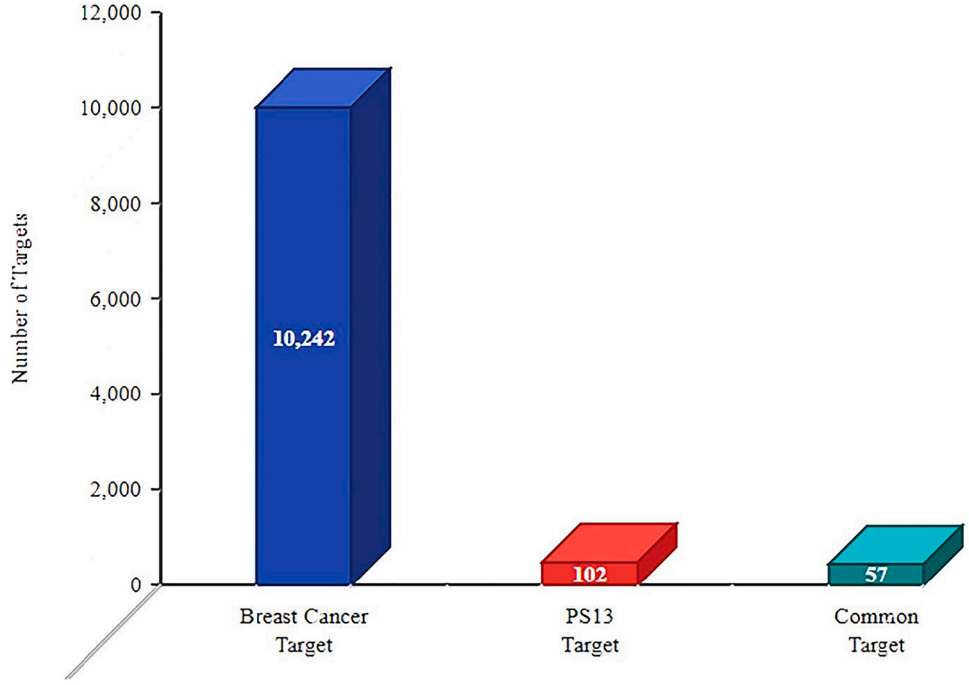

Fig. 1. Bar chart representing the number of identified targets: 10,242 for breast cancer, 102 for compound PS13, and 57 common targets shared between PS13 and breast cancer-associated genes.

with the ability to take into account all the interactions of a compound with a network of molecular targets as opposed to a single target, which is the receptor.

The protein interaction network showed that PS13 selectively binds to ERBB3 while avoiding other EGFR family receptors particularly ERBB3. This finding demonstrated compound specificity directly from the HER2 pathway analysis. The oncogenic pathway-initiating role of ERBB3 depends on its ability to pair up with ERBB family members ERBB2 and ERBB4 thus triggering several dangerous downstream events.

Many signaling proteins including GRB2 and EGF as well as GAB1 and SOS1 together with PLCG1 and MAP2K form the sequence of protein interactions within this network. A vital group of signaling molecules that sustains survival and induces cell growth includes AKT3, STAT5A, HRAS, MAPK1, MAPK8, MAP2K7 and MTOR.

pokus and NRG1, NRG2, NRG3, NRG4 and AREG, EREG, TGFA, HBEGF together with IF4EBP were identified as fundamental ERBB signaling regulators. Regulation occurs in multiple layers through kinase-related proteins that include PTK2, PRKCA, CAMK2A, and PAK4 within the complex network.

JUN and ELK1 together with CDKN1A, CDKN1B and MYC and BAD function as transcription factors and cell cycle regulators that emerged as important downstream targets. The signaling network triggered by ERBB3 also includes CRK, CBL, SRC, SHC2, ABL1, URF-PIK3R3, NCK1, and GSK3B among other interactors.

The study creates an extensive network representation of PS13 as it engages with breast cancer signaling elements thus demonstrating its potential as a multi-targeted inhibitor. Experimental investigations and clinical assessments of PS13 must proceed due to its demonstrated capability to manage important breast cancer-related signaling pathways through identification of 57 common targets Fig. 2.

3.3. Protein analysis

The protein structure stereochemical parameters received evaluation through PROCHECK for quality assessment. The Ramachandran plot analysis showed that 93.6 % of residues occupied regions within the most favoured areas (A, B, L) indicating the high quality of the model. Among the assessed residue regions, a, b, l, p showed an additional presence of 5.5 % and the generously allowed and disallowed regions (~a, ~b, ~l, ~p and XX) contained 0.4 % each. The accepted standards for evaluating 118 high-resolution crystal structures define a trustworthy model as one containing more than 90 % residues in the most favoured regions. The current model exhibits all essential structural components needed for an acceptable and sound configuration.

The protein model contained 236 residues that were neither proline nor glycine along with 17 glycine and 15 proline residues for a total count of 272 residues. The structural quality of the model receives additional support because just one residue exists in the disallowed region.

G-factor analysis served to check stereochemical quality levels. The G-factor average measurement of 0.11 indicates that geometrical distortions are not significant in the model structure. The G-factor evaluation for angles phi-psi (0.05), chi1-chi2 (0.21) and chi1 only (0.15) along with chi3 & chi4 (0.49) revealed satisfactory results. The omega angle displayed an unusual value of −0.54 although it remained inside the acceptable limits and requires careful assessment.

The evaluative metrics regarding main-chain covalent forces showed a favorable compatibility with established standards through their bond length (0.39) and bond angle (0.34) conformity results. The experimental data supports that the stereochemistry of the protein model features proper arrangement and reduced structural irregularities.

The analysis of protein pockets showed ten significant cavities which exhibited unique size features and shell residue compositions. The deepest pocket among all identified openings presented itself as Cleft 1 because it contained 6733.55 Å^3 volume and reached 19.60 Å depth with R1 ratio equality at 5.38. The cleft included sixteen positively charged along with fourteen negatively charged residues and eleven neutrals and thirty-four aliphatic and seven aromatic residues as well as nine proline/glycine residues followed by two cysteine residues. The active site containing a bound ligand (70I 1101[A] with 42 atoms) situated in Cleft 1 makes this pocket the primary active site which possesses both high accessibility and depth suitable for drug development.

Three cleft sections named Cleft 2 and Cleft 3 proved to have intermediate sizes (1231.28 Å^3 and 851.50 Å^3) and typical cavity depths of about 7.9 Å despite having fewer aromatic and charged elements thus revealing probable low affinity for such ligands. Clefts 1–3 contain a wide range of residue types which demonstrate various conducive conditions for ligand attachment.

Most ligand recognition and stabilization happen through hydrophobic interactions because the majority of clefts particularly clefts 1 and 4 have abundant hydrophobic (aliphatic) residues. These research results show that cleft 1 presents itself as an optimal structure for developing drugs through the application of structure-based design

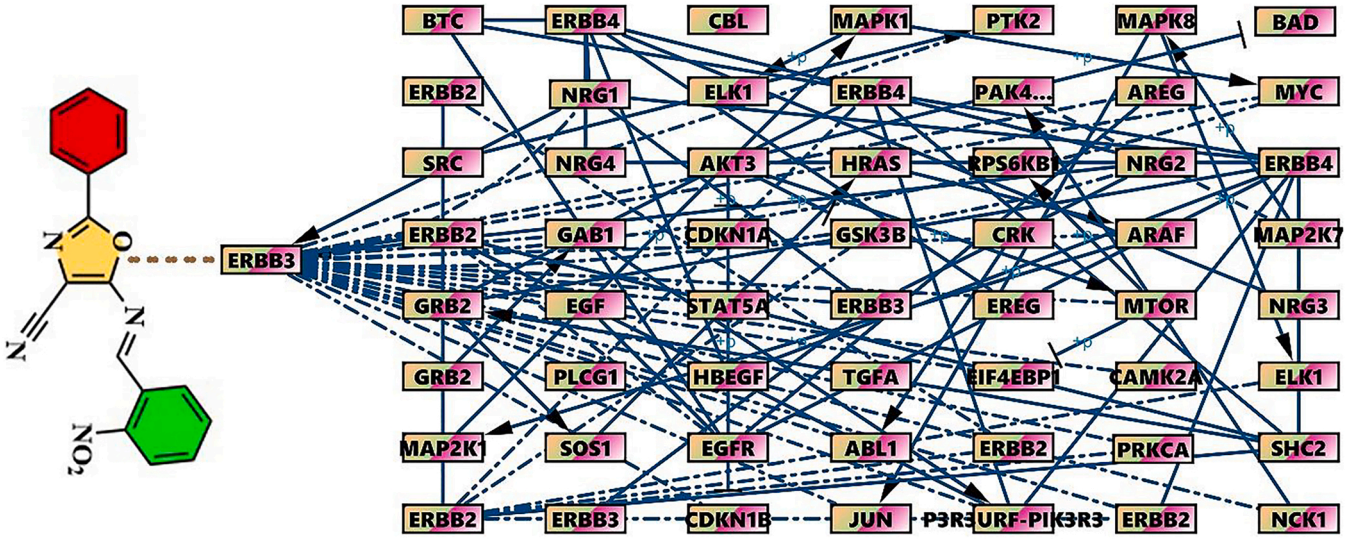

Fig. 2. Network pharmacology interaction map showing PS13 targeting ERBB3 and its associated signalling proteins involved in breast cancer pathways, highlighting downstream mediators, effectors, and cross-linked oncogenic nodes.

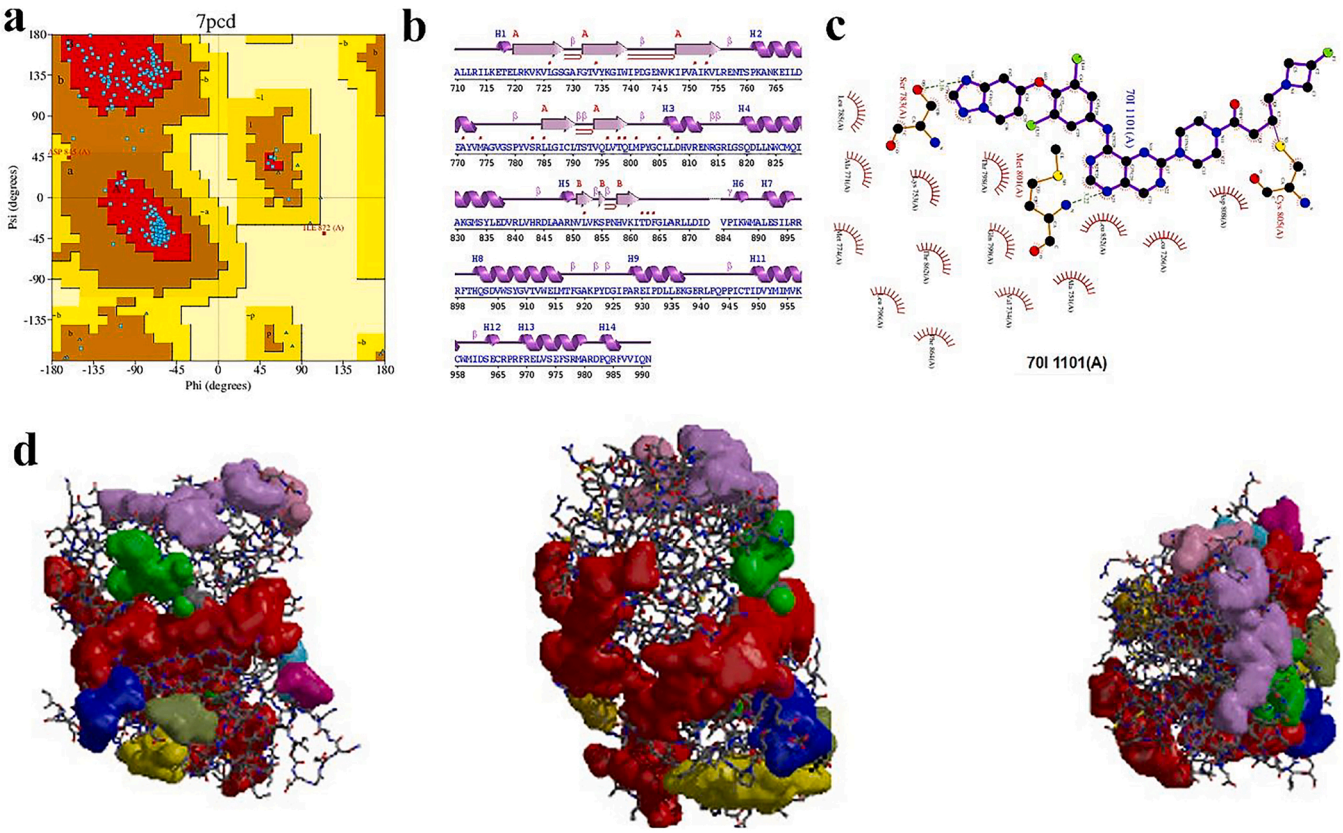

Fig. 3. Structural validation and interaction analysis of 7PCD: (a) Ramachandran plot, (b) secondary structure, (c) 2D ligand interaction map, and (d) surface representation showing binding site regions.

techniques Fig. 3.

3.4. Molecular docking analysis

The Autodock Vina program executed Virtual Screening (VS) to discover potential ERBB3 protein inhibitors that represent suitable targets for breast cancer treatment. The set parameters for virtual screening included an exhaustiveness value of 8 to achieve the best results in terms of accuracy and computational efficiency. The evaluation process involved 25 selected complexes with top scoring affinity which were measured through Vina binding score (kcal/mol). The bioinformatics results showed PS13 together with PS5 and PS6 as the top compounds because they reached –9.5 kcal/mol binding energy this signifies efficient receptor site interaction. The compound PS21 achieved a binding score of –9.4 kcal/mol and seven additional compounds including PS14, PS16, PS17, PS18, PS20, PS22 and PS24 exhibited a comparable score of –9.3 kcal/mol demonstrating their capacity to be potent ERBB3 inhibitors. The binding energies between the compounds PS15, PS1, PS23, PS4 and PS13 and their target amounted to –9.2 kcal/mol thus demonstrating relatively strong binding potentials. The ligands PS12, PS19, PS25, PS2, PS8 recorded binding energies from –9.1 to –9.0 kcal/mol and PS11, PS3, PS9, and PS10 followed with outcomes between –9.0 and –8.9 kcal/mol. Multiple substances showed considerable compatibility with the ERBB3 target according to these research results. Studies utilizing network pharmacology established the key breast cancer targets of PS13 which demonstrated the best docking score alongside its outstanding performance. These ligands demonstrate desirable binding properties and structural characteristics which justify their assessment through in vitro and in vivo clinical tests to determine their utility in breast cancer treatments. The selected top hits serve well for molecular dynamics simulations and pharmacokinetic testing applications. The PDB ID: 7PCD database for ERBB3 allowed researchers to study strong binding relationships between PS13 and the target protein. The PS13 ligand stabilizes its position in the binding pocket by forming hydrogen bonding interactions with Asp863(A), Thr862(A), and Ser863(A) as shown in Figure a of the 2D interaction diagram. Additional stability for the ligand came from hydrophobic binding interactions with Leu800 alongside Val734, Leu736, Phe864 and Met801. The PS13 compound demonstrated excellent binding suitability to the active site (3D binding mode - Figure b) that reflected strong binding affinity. The research demonstrates that PS13 shows strong prospective value as an ERBB3 inhibiting drug which could advance into breast cancer drug development Fig. 4.

3.5. Molecular dynamics analysis

The stability and binding of PS13 with the ERBB3 receptor as revealed in the molecular dynamics (MD) simulations used in the paper has a great support on its anticancer purpose. The main objective of the MD simulations was to determine the stability of the ligand-protein complex in time and to learn the process of how the binding affinity takes place at the molecular level. The findings showed that the PS13-ERBB3 complex preserved a steady conformation during the 500 ns simulation time when there were insignificant variations in the Root Mean Square Deviation (RMSD) of the protein backbone as well as the ligand. This stability implies that PS13 is able to bind the ERBB3 receptor in a strong and stable interaction which is important in its potential use as a targeted anticancer agent. The MD simulation also indicated that PS13 was able to restrict the movement of the key residues in the binding pocket especially Leu 736, Val 734, Lys 753, and Phe 864. These residues comprise the active site of the receptor and are necessary to the active signalling of the receptor in oncogenic processes. PS13 because of the combination of hydrogen bonds, hydrophobic interactions, and water-mediated bridges between these residues, prevents

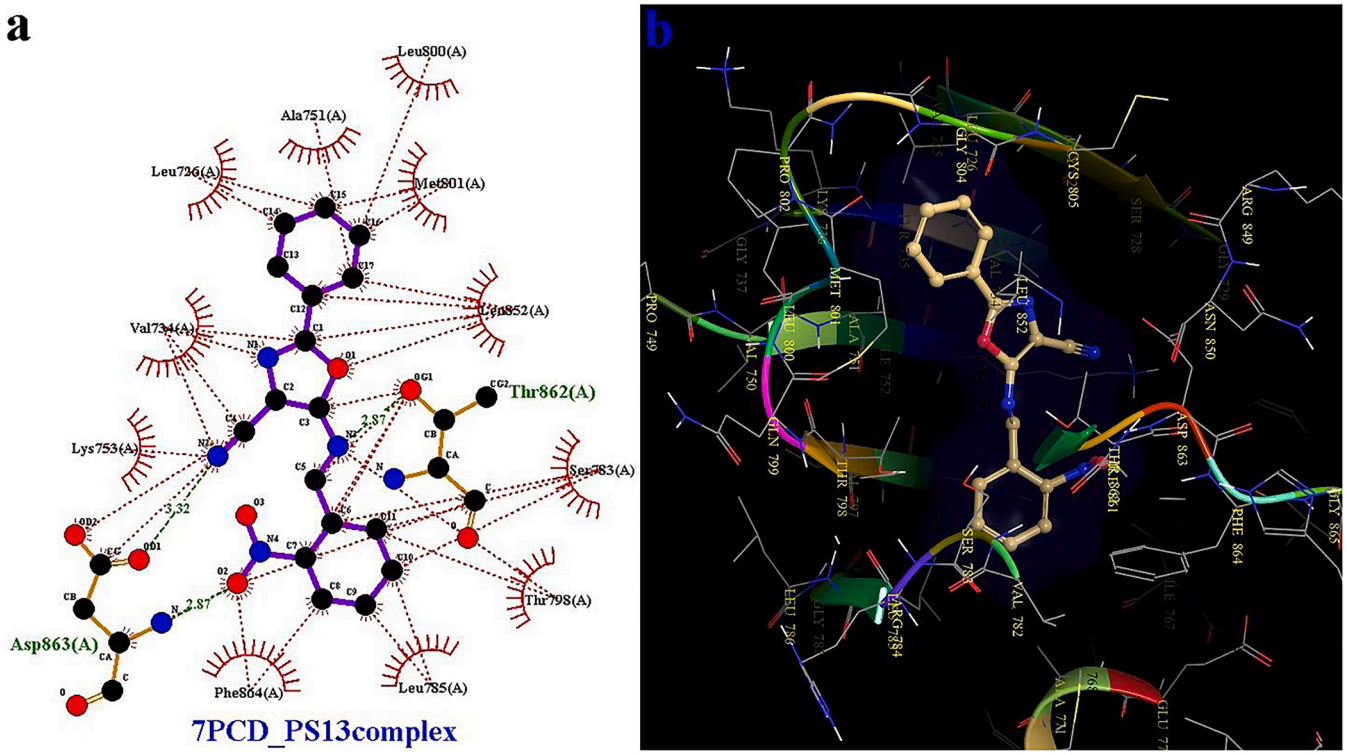

Fig. 4. 2D (a) and 3D (b) interaction diagrams of PS13 with ERBB3 (PDB ID: 7PCD), showing hydrogen bonds, hydrophobic contacts, and binding site stabilization within the active pocket.

the receptor to trigger downstream signalling pathways which promote survival and growth of tumours. Also, the MD outcomes were supplemented with an in-depth overview of the interaction of the ligand with the ERBB3 receptor which revealed that PS13 had always exhibited positive binding interactions with the key residues of the receptor. This shows that PS13 has the ability of disrupting ERBB3 mediated signalling pathways which enhance cancer cell survival and metastasis. The stability and low structural changes in the process of simulation also point towards the aptness of PS13 as a lead compound in attacking ERBB3 in breast cancer (Fig. 5a-e). Finally, the MD simulations also support the anticancer properties of PS13 by showing that it can establish a stable and efficient complex with ERBB3, which helps it to prevent cancer-stimulating signalling networks.

3.6. ADMET analysis

Research conducted with SwissADME examined the physical characteristics as well as pharmacokinetic behavior and drug-likeness attributes of compound PS13. PS13 maintains a molecular weight of 318.29 g/mol and its molecular formula $C_{17}H_{10}N_4O_3$ suits the oral drug parameters well. The compound contains 4 rotatable bonds, 6 hydrogen bond acceptors and no hydrogen bond donors and a topological polar surface area (TPSA) value of 108.00 Å^2 indicating it achieves an ideal balance between solubility and permeability. Numerous water solubility

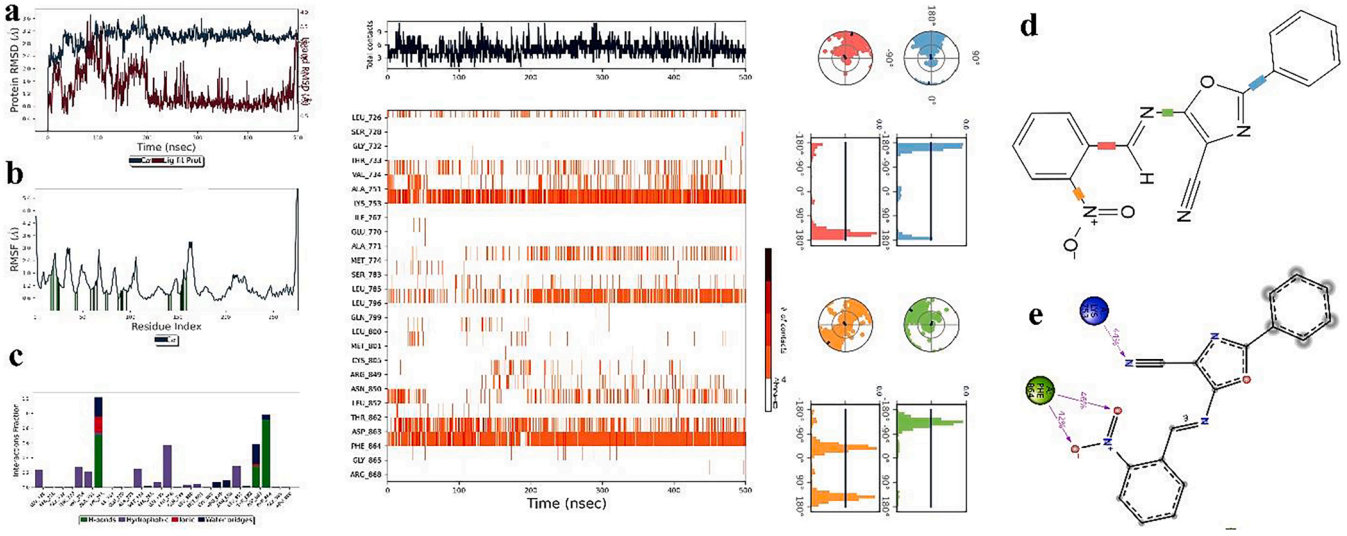

Fig. 5. Molecular dynamics and interaction analysis of PS13 with ERBB3 showing RMSD, RMSF, interaction maps, torsional stability, pharmacophore features, and 2D/3D binding interactions.

forecasts by ESOL, Ali, and SILICOS-IT models point to average solubility potential because the models project log S values of –4.28, –5.46, and –5.81. The data indicates the compound has enough aqueous solubility for oral administration even though its overall solubility level is not very high. The bloodstream distribution of PS13 shows promising gastrointestinal absorption properties but inadequate blood-brain barrier crossing ability which enables its use to target peripheral sites in breast tissue ERBB3. PS13 demonstrates a non-P-gp substrate behavior thus lowering the chance of drug resistance and efflux occurrence. The predictions indicate that PS13 inhibits three main cytochrome P450 enzymes (CYP1A2, CYP2C19, and CYP2C9) which requires closer examination regarding possible drug–drug interactions. The favorable value of consensus Log P = 2.73 indicates drug bioavailability should perform well. Drugs-Likeness criteria of Lipinski, Ghose, Veber, Egan, and Muegge proved non-violating for this chemical compound. One issue with lead-likeness requirements became identified through XLOGP3 values exceeding 3.5 and Brenk alert signals detected imine group and nitro group and oxygen-nitrogen single bond systems because they might represent potential drug-related problems. Research findings indicate that PS13 has a bioavailability score of 0.55 and a synthetic accessibility score of 3.55 which together demonstrate that the compound possesses positive drug-like properties and exhibits moderate accessibility to synthesis. Several laboratory tests demonstrate that PS13 possesses the potential to serve as a first-choice substance for treating breast cancers that target ERBB3 receptors Fig. 6.

3.7. Density functionality theory

A quantum chemical calculation of PS13 determined its HOMO–LUMO energy gap to assess electronic behavior and chemical reactive potential. Quantum chemical analysis determined the HOMO energy at −8.30 eV while LUMO energy was found at −6.03 eV resulting in a −2.27 eV energy gap. PS13 demonstrates broad electron donating and accepting power because of its narrow energy gap which should boost its biological activity when interacting with target proteins. The medium-sized energy gap demonstrates stability balance with reactivity features which establishes this compound as a promising candidate in drug development especially for anticancer therapy through electron transfer processes Fig. 7. The DFT results are informative on the electronic characterizations of the anticancer action of the synthesised products. The mid HOMO-LUMO energy difference is an indicator of the optimum balance between the stability and reactivity of the molecule and this promotes desirable interactions with biological targets. The presence of high HOMO energy indicates high efficiency of the electron donating property, which is in favour of a strong receptor-affinity whereas the presence of low LUMO energy indicates high efficiency of acceptance of the electron density within the ERBB3 binding pocket. These properties have the potential to strengthen hydrogen bonding, p-p interactions as well as the overall ligand-receptor affinity, as a part of cellular growth inhibition. In that way, the results of DFT complement the experimental findings of cytotoxicity, which confirms the therapeutic efficacy of these new oxazole derivatives.

5-amino-2-phenyloxazole-4-carbonitrile 1 l

Yield: 85 %; m.p.: 182–184 °C. IR (cm^{-1}): 337 (NH), 3021 (Ar-CH), 2972 (Ali-CH), 1624 (C═N), 1626 (C═C), 1024 (C-O-C).

^{1}H NMR (400 MHz, DMSO-d_6) δ 7.95 (brs, 2 H), 7.73 (m, 2 H), 7.43 (m, 2 H) (Figure S1).

^{13}C NMR (100 MHz, DMSO-d_6) δ 162.9, 149.8, 130.3, 129.1, 126.0, 125.1, 115.6, 84.3 (Figure S2).

MS (EI) *m/z*: 185 (M^+). *Anal.* Calcd for $C_{10}H_7N_3O$: C, 64.86; H, 3.81; N, 22.69; Found: C, 64.84; H, 3.83; N, 22.67 (Figure S3).

HPLC- retention time of 2.51 min (Figure S4).

5-((2-nitrobenzylidene)amino)-2-phenyloxazole-4-carbonitrile PS13

Yield: 87 %; m.p.: 193–195 °C. IR (cm^{-1}): 3060 (Ar-CH), 2921 (Ali-CH), 1520 (N-O), 1613 (C═N), 1019 (C-O-C).

^{1}H NMR (400 MHz, DMSO-d_6): δ 9.46 (brs, 1 H), 8.35 (m, 2 H), 8.14 (m, 3 H), 8.14 (m, 3 H), 7.78 (m, 1 H), 7.71 (m, 2 H), 7.66 (m, 1 H) (Figure S5).

^{13}C NMR (100 MHz, DMSO-d_6) δ 159.3, 154.5, 149.7, 149.1, 133.1, 131.2, 129.1, 128.1, 126.6, 125.6, 125.0, 124.3, 122.9, 113.3 (Figure S6).

MS (EI) *m/z*: 318 (M^+). *Anal.* Calcd for $C_{17}H_{10}N_4O_3$: C, 64.15; H, 3.17; N, 17.60; Found: C, 64.18; H, 3.18; N, 17.62 and HPLC- retention time of 3.20 min (Figure S7).

Successful synthesis of 5-((2-nitrobenzylidene)amino)-2-phenyloxazole-4-carbonitrile (PS13) resulted in an excellent yield of 87 % due to the effective condensation reaction between 5-amino-2-phenyloxazole-4-carbonitrile and 2-nitrobenzaldehyde. The compound achieved high purity based on its sharp melting point range from 193 to 195 ° Celsius.

Ultraviolet IR spectroscopy measurements showed two essential peak clusters at 3060 cm^{-1} and 2921 cm^{-1} which represented aromatic and aliphatic C–H bond stretching. Strong absorption at 1520 cm^{-1} existed for the nitro (N–O) group accompanied by C═N stretching at 1613 cm^{-1} to show that Schiff base formation was successful. A multiplet range from 7.32 to 7.93 ppm contained nine aromatic protons in addition to an azomethine proton signal (CH═N) at 4.143 ppm in ^{1}H NMR. The $^{1\ 3}$C NMR spectrum revealed peaks from δ 123.2 to δ 148.4 ppm which indicated aromatic carbons together with dedicated peaks at δ 160.2 ppm for imine carbon and δ 117.2 ppm for the nitrile carbon. The measured molecular weight of *m/z* 318 corresponded to the theoretical peak value. The obtained elemental analysis data verified the molecular formula $C_{17}H_{10}N_4O_3$ by matching predicted outcomes. All spectral data and analytical measurements proved the successful synthesis and proper structural framework of PS13. The

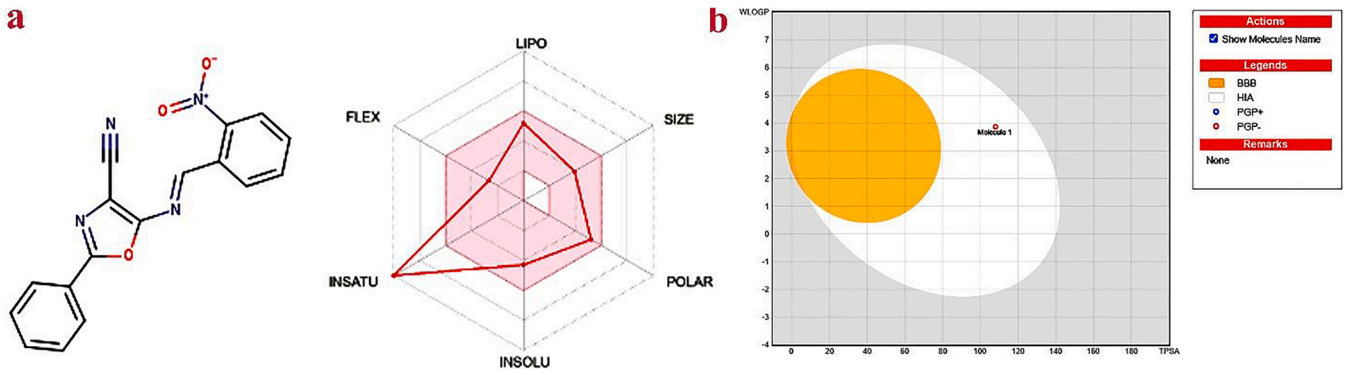

Fig. 6. (a) Structure and bioavailability radar plot of the compound indicating optimal physicochemical properties. (b) BOILED-Egg model predicting gastrointestinal absorption and blood-brain barrier permeability of the compound.

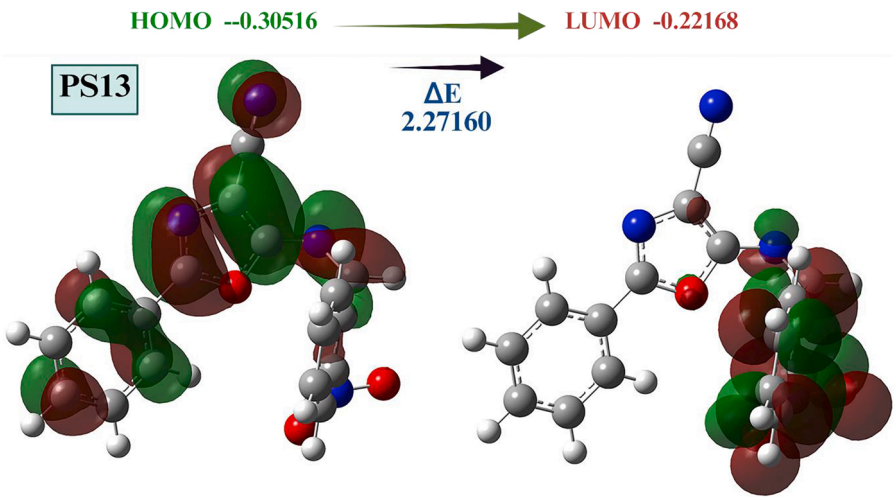

Fig. 7. HOMO–LUMO energy orbital distribution of PS13, showing electron density transitions with an energy gap (ΔE) of 2.2716 eV, indicating electronic reactivity and potential biological interaction sites.

syntheses of PS13 occurred through analysis of 5-amino-2-phenyloxazole-4-carbonitrile (1 l) against the final product. NMR results showed the signal at δ 4.143 ppm as the imine proton of PS13 which did not exist in 1 l indicating successful Schiff base formation. The IR spectral analysis showed two significant changes which confirmed condensation because the NH_2 stretch at 337 cm^{-1} vanished yet both C═N and nitro group at 1613 cm^{-1} and 1520 cm^{-1} emerged. The mass spectrometry analysis showed identical molecular ion peak (*m/z* 318) and it confirmed the molecular weight was consistent between samples. Spectral analyses as well as analytical parameters affirmed that 1 l underwent successful conversion into PS13 by producing Schiff base derivative.

The choice of the reported PS13 with nitro and cyano groups is scientifically grounded on the already established role in the pharmacological activity. Nitro groups molecular weight increase the electron-withdrawing ability, which promotes interaction of ligands and receptor, increase hydrogen binding in active sites. Equally, the cyano group offers structural rigidity, enhanced lipophilicity and p-stacking interactions, thus enhancing target affinity and intracellular permeability. All these functionalities together lead to electronic stabilisation, which favours efficient binding with ERBB3. Moreover, both groups have been prominently known in the anticancer drug design as an induction to the apoptosis and growth inhibition. Therefore, they are not accidental, but rather enhance therapeutic potential.

3.8. *PS13-encapsulated SLNs*

Synthesis of PS13-encapsulated SLNs occurred through an oil-in-water microemulsion method. The PS13 loading in SLNs achieved a high efficiency of 81 ± 2.16 % together with a capacity of 8.96 ± 2.16 % Fig. 8.

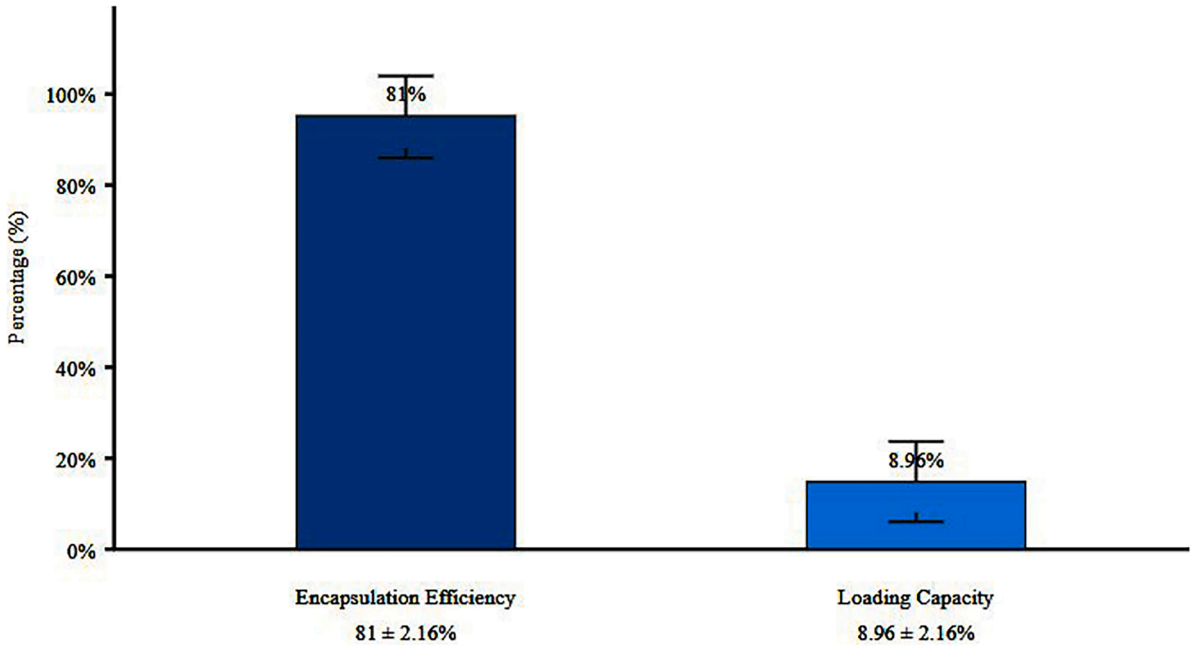

Fig. 8. The encapsulation efficiency and loading capacity of PS13-encapsulated SLNs. The encapsulation efficiency is 81 % ± 2.16 %, while the loading capacity is 8.96 % ± 2.16 %.

3.9. In vitro release of PS13 from SLNs

The experimental evaluation of PS13 release from PS13-encapsulated SLNs occurred through HPLC quantification in two buffer systems including acetate buffer at pH 5.2 and phosphate buffer at pH 7.5 at 30 °C. The research data showed that PS13 released into bloodstream from the SLNs occurred at a measured pace while maintaining controlled kinetics. PS13 release reached 39.217 ± 0.341 % (pH 5.0) but also 42.312 ± 0.231 % (pH 7.2) after 7 h. PS13 shows better release properties at pH 7.5 in phosphate buffer when compared to its release properties in acetate buffer at pH 5.2. The release of PS13 reached its highest point at 55 h under both buffer conditions where the maximum released amounts were measured as 89.231 ± 0.224 % (pH 7.5) and 84.112 ± 0.423 % (pH 5.2) Fig. 9.

3.9.1. Drug release kinetics of PS13-encapsulated SLNs

Studying the drug release attributes of PS13-encapsulated SLNs. The PS13 drug release data underwent evaluation through zero-order, first-order, Higuchi, Korsmeyer-Peppas, and Hixson-Crowell standard models. The researchers performed all kinetic experiments in strictly controlled environments. Each model received statistical determination of its release rate constant combined with its regression coefficient (r^2). A near value of 1 in r^2 shows a more robust correlation between variables. R^2 values at pH 5.2 spanned from 0.9214 to 0.9012 and at pH 7.5 they fell between 0.9524 and 0.9172 which revealed better first-order than zero-order kinetic behavior. Most linear curves except for Korsmeyer-Peppas demonstrated r^2 values greater than 0.92 which indicates their satisfactory fit to the data. Experimental findings demonstrated that PS13 released from SLNs occurred through Fickian diffusion which validated the controlled drug delivery mechanism. The first-order kinetics distribution emerged as the most suitable mechanism for characterizing the drug release patterns according to these kinetic examinations and (Et) PSA data. The nanoparticles exhibited uniform breakdown while releasing their contents steadily according to results Fig. 10.

3.10. Stability studies of PS13-encapsulated SLNs

The UV absorption spectra evaluation for PS13-encapsulated SLNs under stabilizing conditions between 200–350 nm resulted in recorded absorbance data to create a graph of PS13-encapsulated SLNs. Different stabilizing solutions influenced the wavelength at which SLNs absorbed the maximum amount of light. Strong absorption occurred in the high ionic strength solution of 10 % NaCl (w/v) which caused the measurement peak to appear at 252 nm. The wavelength maximum (λmax) of SLNs stabilized through 0.5 % BSA (w/v) solution reached 263 nm because of possible protein binding effects. The spectrophotometric spectra recorded for PS13-encapsulated SLNs at both pH 5.2 acetate buffer and pH 7.5 phosphate buffer maintained a uniform λmax value at 281 nm. The absorbance spectrum of SLNs moved to 281 nm when placed in simulated gastric juice indicating that stomach conditions could affect their absorbance pattern Fig. 11.

3.10.1. LC-MS Analysis of PS13-encapsulated SLNs

The analyses using Liquid Chromatography-Mass Spectrometry (LC-MS) detected specific retention times alongside MS peaks from the active components of PS13-encapsulated SLNs. The extracted PS13 appeared at 3.2 min with a mass-to-charge ratio of 318.29 $[M+H]^+$ during LC-MS analysis Fig. 12.

3.10.2. FE-SEM analysis of PS13-encapsulated SLNs

The FE-SEM image shows PS13-encapsulated SLNs exist as rounded structures indicating successful encapsulation measures. The microscopic images display PS13-encapsulated SLNs having a smooth surface together with consistent dimensions which signifies the successful synthesis procedure and encapsulation achievement. Stability and production reproducibility improve significantly because of the minimal amount of agglomeration that is detected alongside smooth surfaces. The uniform dimensions of these particles indicate achievement of precise preparation methods which ensure therapeutic consistency. Long-term drug release becomes possible due to the smooth nanoparticle structure which features few visible flaws to block immediate

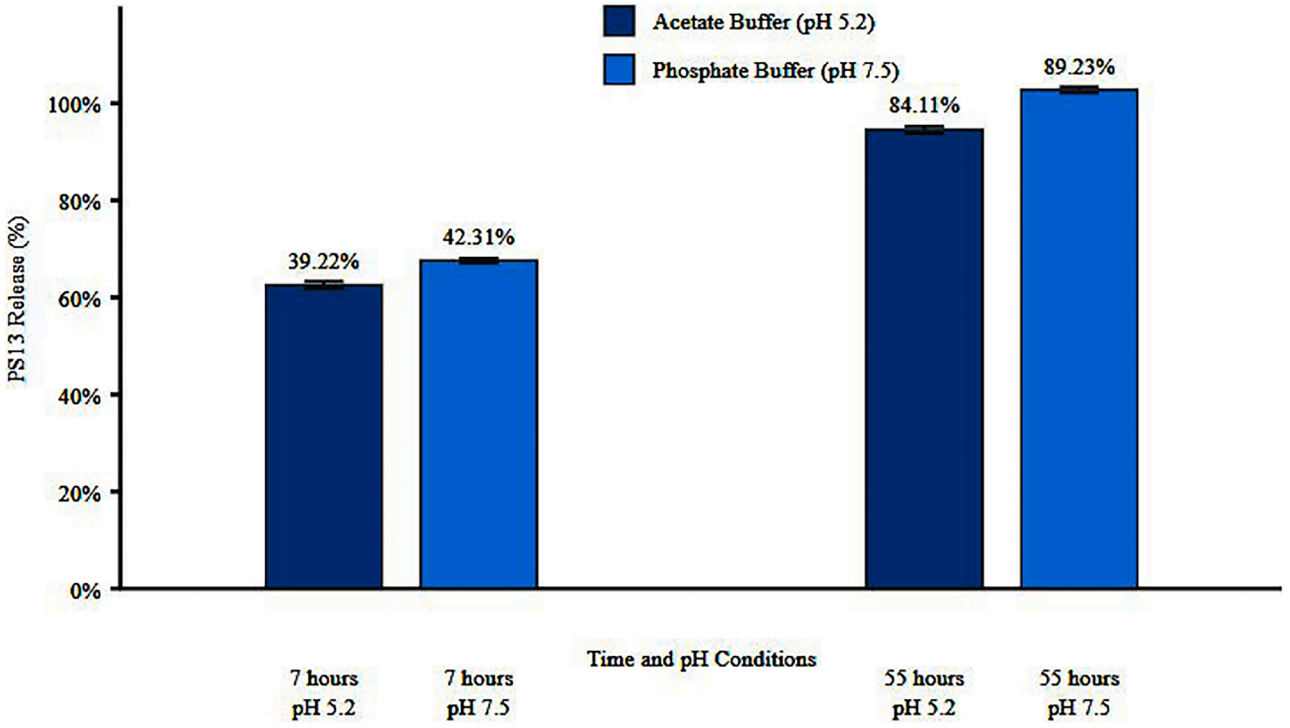

Fig. 9. The release of PS13 under different pH conditions (acetate buffer at pH 5.2 and phosphate buffer at pH 7.5) over 7 and 55 h. The release increases with time and pH.

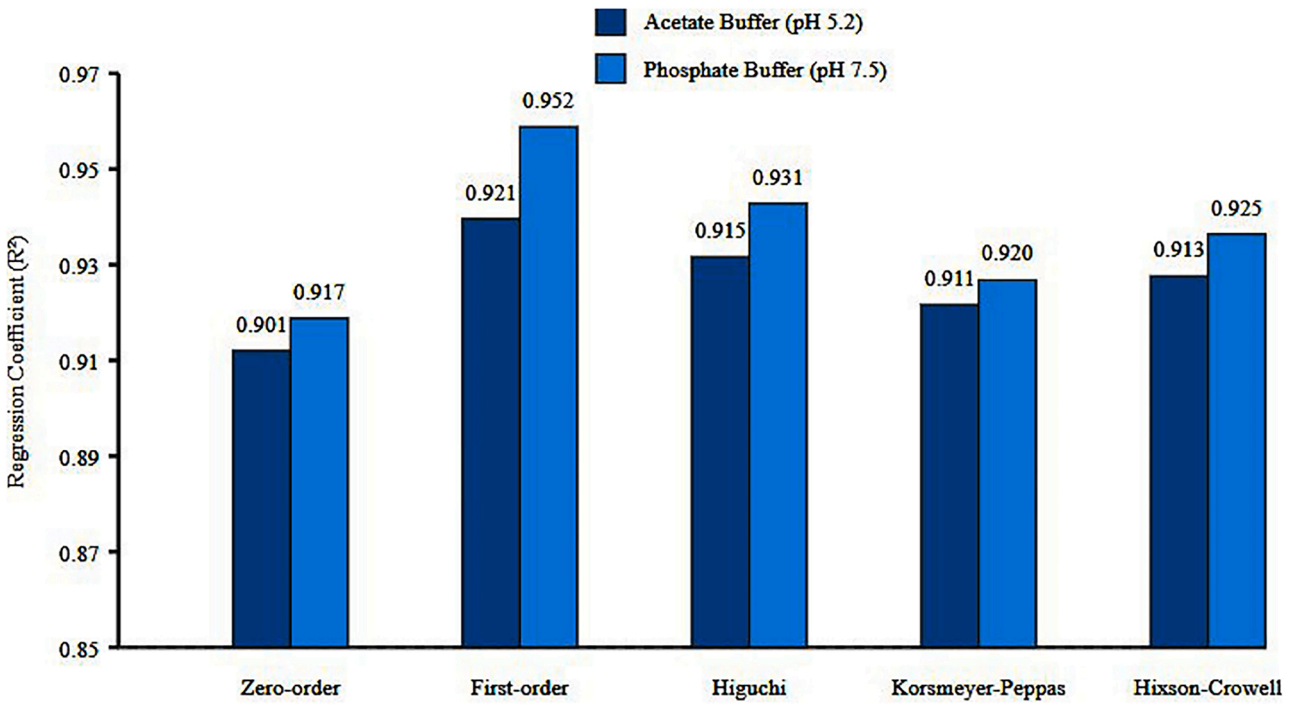

Fig. 10. The regression coefficients (R^2) for various drug release models (Zero-order, First-order, Higuchi, Korsmeyer-Peppas, and Hixson-Crowell) in acetate and phosphate buffers at pH 5.2 and 7.5.

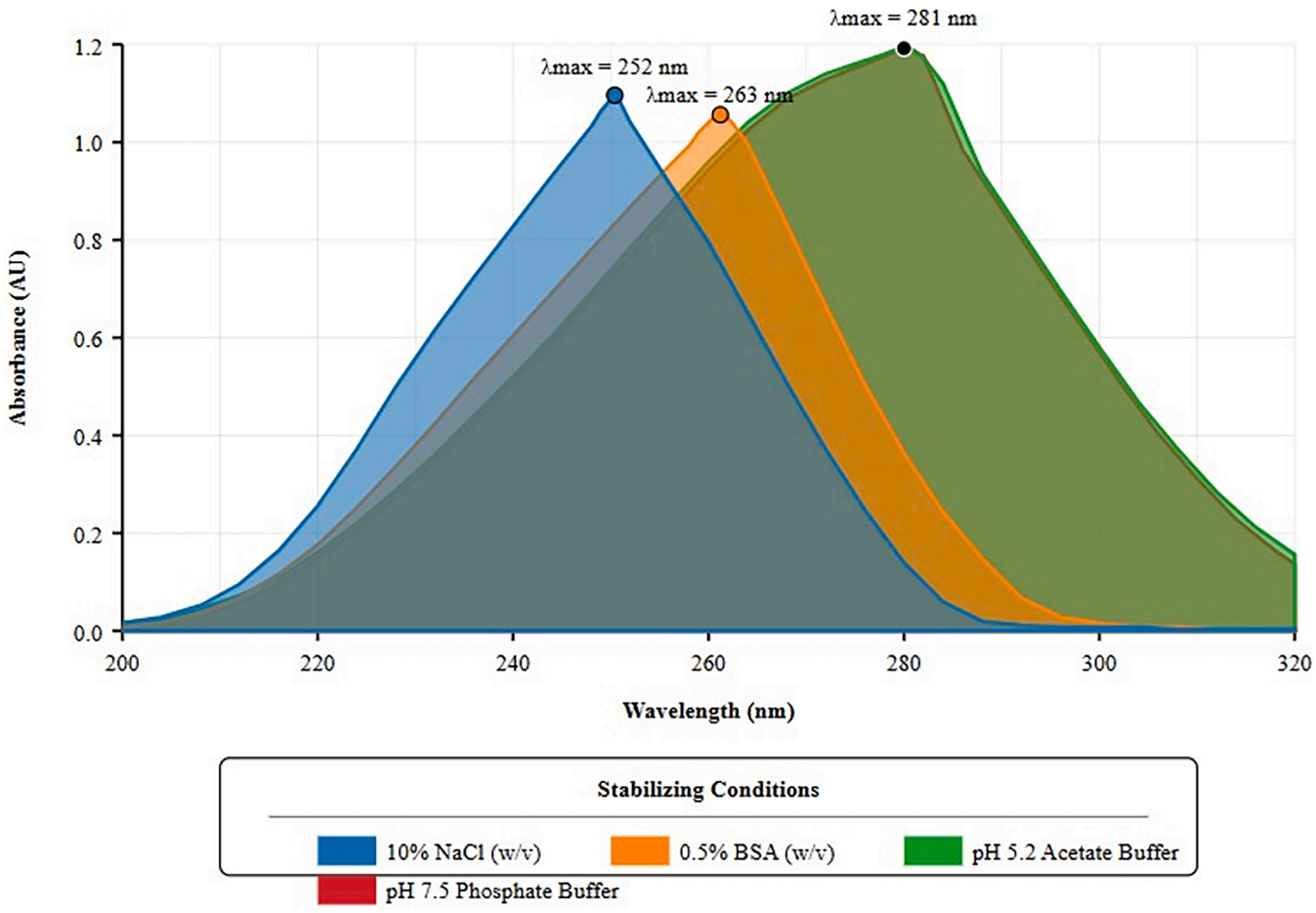

Fig. 11. The absorbance spectra of PS13 under different stabilizing conditions: 10 % NaCl, 0.5 % BSA, pH 7.5 phosphate buffer, and pH 5.2 acetate buffer, with corresponding λmax values indicated.

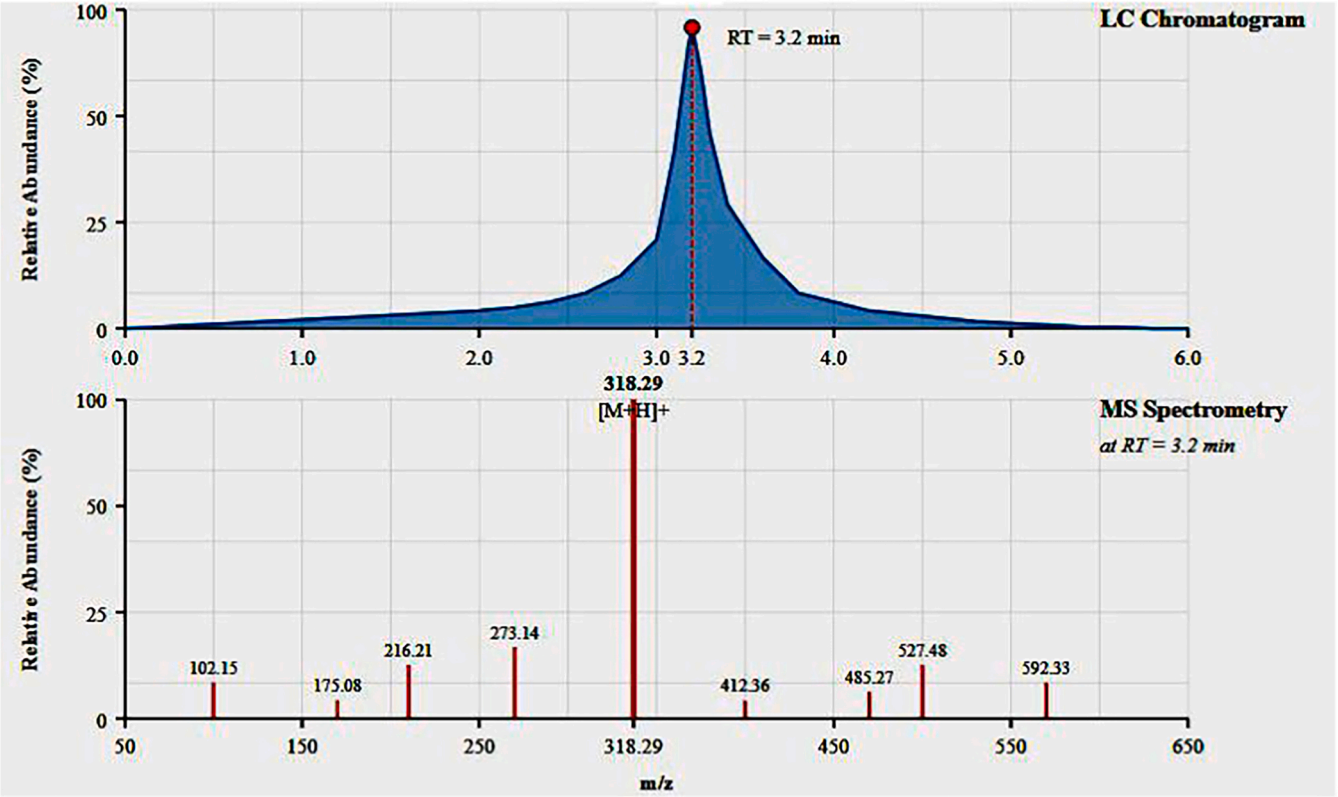

Fig. 12. the LC chromatogram of PS13, with a retention time (RT) of 3.2 min, and the corresponding MS spectrum at RT 3.2 min, identifying the molecular ion peak at *m/z* 318.29.

drug release. The drug encapsulation method achieved high efficiency because the analysis detected neither drug loss nor chemical breakdown which shows improved drug stability together with enhanced bioavailability. The physical characteristics demonstrated by PS13-encapsulated SLNs demonstrate their suitability to act as an effective drug delivery system based on the FE-SEM findings Fig. 13.

3.10.3. FTIR analysis of PS13-encapsulated SLNs

PS13 shows absorbance peaks in its IR spectrum that represent its fundamental functional group structures in the spectrum. The Aro–CH stretching vibrations are confirmed by a wide band between 3005 cm^{-1} which indicates the presence of Aro–CH. The stretch of C-H bonds in alkyl groups occurs around the 2854 cm^{-1} wavelength. Aromatic ring structures can be identified through C═N stretching peaks at 1680 cm^{-1} together with C═C stretching vibrations occurring between 1457 cm^{-1} . The 1285 cm^{-1} spectral range contains signals from C–O bonds that exist either as alcohols or ethers and C–H bending from aromatic rings takes place near 721 cm^{-1} Fig. 14.

3.11. In vitro anti-breast cancer activity

PS13 underwent an MTT assay examination for its cytotoxic capacity over a range of increasing concentrations starting from 6.25 μg to 100 μg when tested against cancer cells. An optical density reading taken at 570 nm served to evaluate the cell survival percentage. The viability of cancer cells decreased in direct proportion to increasing concentrations of PS13 solution according to the presented data. When the cell culture received 6.25 μg PS13 concentration it maintained a high cell viability average at 78.45 % indicating low cytotoxic effects. The cell viability levels declined sharply from 78.45 % at 6.25 μg to 67.22 % at 12.5 μg and then plummeted to 60.18 % when using 25 μg concentration. The toxic effect on cells intensified as the solution concentrations increased. The research data indicates that cell surviving rates declined from 51.94 % at 50 μg to 44.75 % at 100 μg which demonstrated a clear cytotoxicity pattern. The minimal standard deviation between replicates showed that the assay achieved high reproducibility and reliability in its results. Experimental results showed PS13 required 60.27 μg to reach 50 % cell inhibition under the experimental conditions (IC_{50}). The microscopic examination of treated cells depicted in the image backed up the recorded results. Cells in the control group exhibited dense and healthy look with no morphological disruptions. The application of increasing amounts of PS13 solution led to systematic decline of cell density and morphological deterioration in the culture plate. A minimal amount of cellular contraction together with reduced cell binding occurred at 6.25 μg and 12.5 μg concentrations of PS13 treatment. The treatment with 25 μg and 50 μg concentrations resulted in heightened morphological changes through diminished cell cells and distortion of their distinctive boundaries. The 100-μg concentration exposed severe cell damage through its production of cellular debris and its destruction of standard cell patterns and structure. The cytotoxic properties of PS13 demonstrated by this investigation should be exploited in future studies due to their cell death mechanisms whose underlying mechanism needs clarification. The investigation using MTT assays alongside microscopy observations has proven that PS13 demonstrates substantial anticancer properties through dosage-dependent effects Fig. 15.

4. Discussion

The present study explored the multifaceted anticancer potential of the oxazole derivative PS13 against ERBB3-positive breast cancer cells and demonstrated a compelling integration of computational, formulation, and in-vitro approaches. Molecular docking revealed a high level of affinity to ERBB3 with binding score of −9.5 kcal/mol with significant hydrogen bonding and hydrophobic interactions in the active site and indicated that PS13 has reacted with the receptor domains that affect downstream signalling. Molecular dynamics simulation also indicated

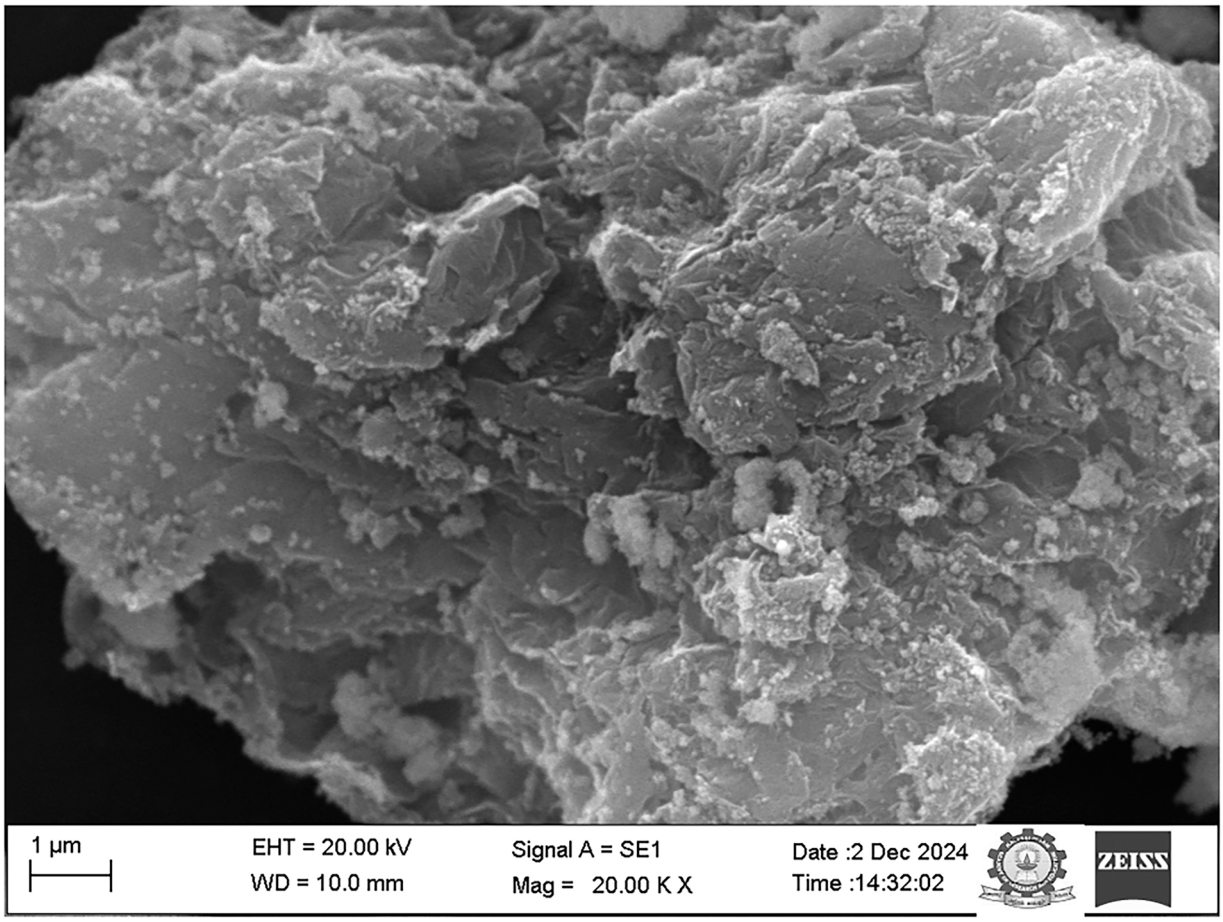

Fig. 13. The figure shows an FE-SEM image of PS13-encapsulated SLNs at a magnification of 20,000x, with a scale bar representing 1 µm. The image illustrates the surface morphology of the nanoparticles.

that the formation of a stable ligand-protein complex with minimal RMSD fluctuations over 500 ns occurred and indicated structural rigidity as well as a positive thermodynamic stability. The pharmacophore mapping added to these findings and emphasised hydrogen bonding and p-p stacking as the main factors of a stable binding. The biological potency was indicative of a moderate HOMO-LUMO gap (-2.27 eV) that was proposed by electron density analysis using DFT, which indicated a balance in its chemical stability and reactivity. PS13 was predicted to be a promising drug-like scaffold that had good properties of absorption and safety, even though cytochrome P450 interactions should be further explored. The attachment of PS13 to solid lipid nanoparticles allowed achieving a high level of entrapment efficiency (81 +/- 2.16) and superior release kinetics, especially at physiological conditions, demonstrating its potential to be used in targeted renal delivery of drugs. A biological relevance was demonstrated in vitro by finding that dose dependent growth inhibition IC_{50} 60.27 ± 0.04 µg/mL) and typical apoptotic morphology occurred in MCF-7 cells during cytotoxicity studies. All these results show that PS13 is a strong lead molecule that has the potential to address the constraints of conventional therapy by integrating ERBB3 inhibition with effective nano-enabled delivery.

5. Conclusion

The article introduces PS13 as a prospective oxazole-based therapeutic candidate to treat ERBB3-driven breast cancer, which is backed by computational, formulation, and cellular analysis. The in-silico binding affinity, which was corroborated by docking and molecular dynamics simulation, indicated that PS13 has the ability to successfully occupy the active pocket of ERBB3 and has the ability of stable ligand-receptor interactions overtime. These structure characteristics imply PS13 has an opportunity to affect ERBB3-mediated signalling cascades that play a role in tumour development, cell growth, and metastasis. To supplement such outcomes, DFT computations showed that the system had favourable electronic features such as sufficient molecular stability and reactivity to allow biological activity. Favourable ADMET profile which includes reasonable oral bioavailability, non-P-gp efflux and desirable physicochemical properties indicates that the compound has translational potential. PS13-loaded SLNs were developed further, which increased its therapeutic appropriateness as indicated by high encapsulation ability, good dispersibility and controlled, pH-responsive release kinetics. Another benefit of the SLN platform to PS13 is that it should enhance bioavailability and reduce premature clearance, which will place PS13 in a better position to perform well in vivo. The anticancer response of MCF-7 cells was attested in in vitro tests through evaluations of the presence of significant dose-dependent cytotoxicity and apoptotic morphological alterations. All in all, this paper highlights the plausibility of PS13 as an effective lead compound in the breast cancer treatment of ERBB3. Its combined functionality; significant receptor binding, good drug-likeness, sustained nanoformulation discharge, and strong anticancer action.

Authors contribution

JX, DZ carried out formal analysis, validation, funding obtained, design and wrote the original manuscript. KR, MD, NK performed analysis the data. PT, SM, SW, WZ contributed to the study's conception, design, supervision, validation, visualization and proofread it. All the authors have read and approved the manuscript for submission.

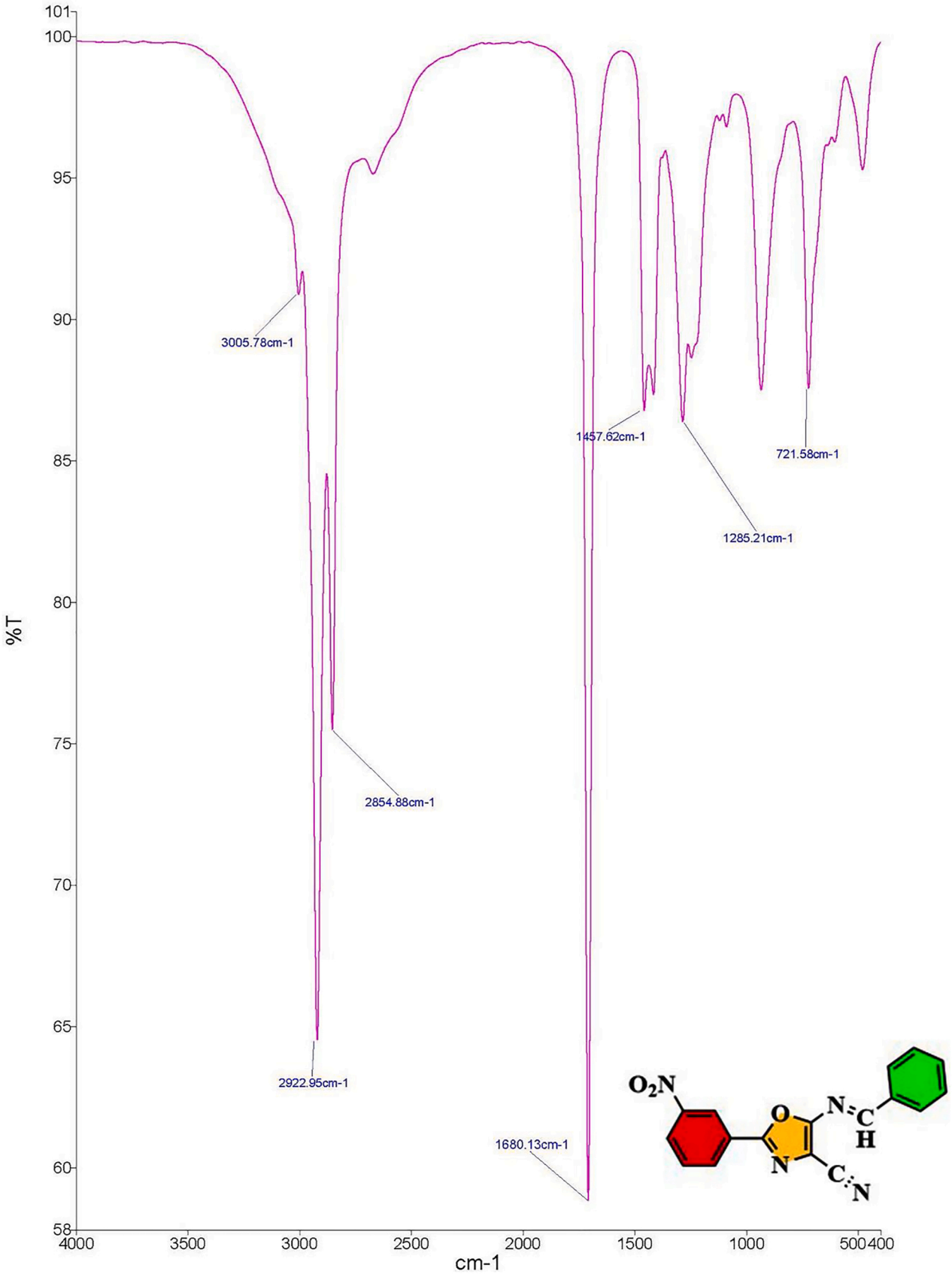

Fig. 14. The FTIR spectrum of PS13, highlighting key absorption peaks at various wavenumbers, including 3005.76 cm^{-1} , 1457.62 cm^{-1} , and 2854.88 cm^{-1} , with the chemical structure inset.

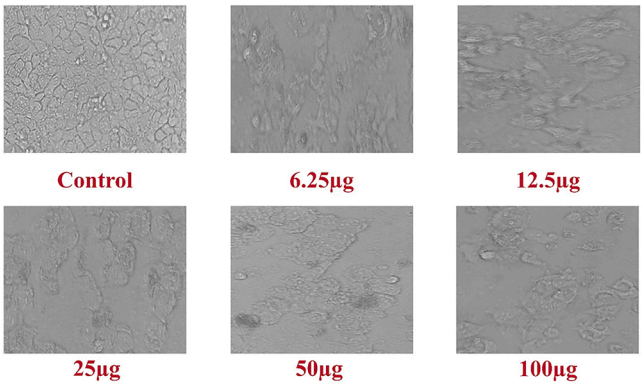

Fig. 15. Microscopic images showing dose-dependent cytotoxic effects of PS13 on cancer cells at various concentrations, with progressive loss of cell integrity and morphology from 6.25 µg to 100 µg.

CRediT authorship contribution statement

Dongwei Zhu: Writing – review & editing, Writing – original draft, Formal analysis, Data curation, Conceptualization. **Mangirish Deshpande:** Writing – review & editing, Writing – original draft, Resources, Project administration, Methodology. **Jianxing Xu:** Writing – review & editing, Writing – original draft, Visualization, Validation. **Selvaraj Muthusamy:** Writing – review & editing, Writing – original draft, Software, Resources. **Siyi Wu:** Writing – review & editing, Writing – original draft, Visualization, Validation, Supervision. **Natarajan Kiruthiga:** Writing – review & editing, Writing – original draft, Investigation, Formal analysis, Data curation. **Panneerselvam Theivendren:** Writing – review & editing, Writing – original draft, Visualization, Validation, Supervision. **RAJALAKSHMI KANAGARAJ:** Writing – review & editing, Writing – original draft, Resources, Project administration, Methodology. **Weizhong Zhao:** Writing – review & editing, Writing – original draft, Project administration, Methodology, Investigation.

Declaration of Competing Interest

The authors declare that they have no known competing financial interests or personal relationships that could have appeared to influence the work reported in this

Acknowledgements

JX thanks to Changzhou Municipal Science and Technology Bureau (CJ2024003, CJ20244004), DZ thanks to the National Natural Science Foundation of China (82202001) and Postdoctoral Science Foundation of China (2024M761196) for the financial supports.

Appendix A. Supporting information

Supplementary data associated with this article can be found in the online version at doi:10.1016/j.compbiolchem.2025.108859.

References

Bansode, P., Patil, P., Choudhari, P., Bhatia, M., Birajdar, A., Somasundaram, I., Rashinkar, G., 2019. Anticancer activity and molecular docking studies of ferrocene tethered ionic liquids. J. Mol. Liq. 290, 111182. ⟨https://www.sciencedirect.com/science/article/abs/pii/⟩S01677 322 19314266.

Bansode, P., Pore, D., Tayade, S., Patil, S., Choudhari, P., Rashinkar, G., 2023. Remarkable anti-breast cancer activity and molecular docking studies of ferrocene tethered pyrimidobenzothiazoles and pyrimidobenzimidazoles. Results Chem. 5, 100758. https://doi.org/10.1016/j.rechem.2022.100758.

Chen, C., Wang, X., Chen, W., Liu, Q., Wang, L., 2025. Encapsulation of phenolic acids within food-grade carriers systems: a systematic review. Crit. Rev. Food Sci. Nutr. 65, 2765–2784. ⟨https://www.tandfonline.com/doi/abs/10.1080/10408398.2024.2350616⟩.

Cianciosi, D., Forbes-Hernandez, T.Y., Ansary, J., Gil, E., Amici, A., Bompadre, S., Simal-Gandara, J., Giampieri, F., Battino, M., 2020. Phenolic compounds from Mediterranean foods as nutraceutical tools for the prevention of cancer: the effect of honey polyphenols on colorectal cancer stem-like cells from spheroids. Food Chem. 325, 126881. ⟨https://www.sciencedirect.com/science/article/abs/pii/S0308814620307433⟩.

Dinesh, B.G.H., Bandral, S.K., Sadashivappa, N.M., Ganjipete, S., Ammunje, D.N., Kunjiappan, S., Theivendren, P., Jays, J., Pavadai, P., 2025. Targeting the PI3K pathway: advancements and achievements in breast cancer therapy. Curr. Pharm. Des. ⟨https://www.benthamdirect.com/content/journals/cpd/10.2174/0113816128357976250122042633⟩.

Fan, J., Liao, Y., Zhao, Y., Wan, J., Wei, Y., Ouyang, Z., 2025. A CYP450 monooxygenase MaCYP82C169 discovered from mulberry leaves catalyzes the methyl oxidation reaction in 1-deoxynojirimycin biosynthesis. Food Biosci. 66, 106177. ⟨https://www.sciencedirect.com/science/article/abs/pii/S2212429225003530⟩.

Gajare, S.P., Bansode, P.A., Patil, P.V., Patil, A.D., Pore, D.M., Sonawane, K.D., Dhanavade, M.J., Khot, V.M., Rashinkar, G.S., 2021. Anticancer, Antibacterial and Hyperthermia Studies of a Caffeine-Based N-Heterocyclic Carbene Silver Complex Anchored on Magnetic Nanoparticles. ChemistrySelect 6, 1958–1968. https://doi.org/10.1002/slct.202004139.

Gan, C., Liu, Q., Zhang, Y., Shi, T., He, W.-S., Jia, C., 2022. A novel phytosterols delivery system based on sodium caseinate-pectin soluble complexes: improving stability and bioaccessibility. Food Hydrocoll. 124, 107295. ⟨https://www.sciencedirect.com/science/article/abs/pii/S0268005X21007116⟩.

Kunjiappan, S., Panneerselvam, T., Pavadai, P., Balakrishnan, V., Pandian, S.R.K., Palanisamy, P., Sankaranarayanan, M., Kabilan, S.J., Sundaram, G.A., Tseng, W.-L., 2024. Fabrication of folic acid-conjugated pyrimidine-2 (5H)-thione-encapsulated curdlan gum-PEGamine nanoparticles for folate receptor targeting breast cancer cells. Int. J. Biol. Macromol. 277, 134406. ⟨https://www.sciencedirect.com/science/article/abs/pii/S0141813024052⟩, 115.

Liu, H., Liang, J., Ye, X., Huang, M., Ma, L., Xie, X., Liu, D., Cao, H., Simal-Gandara, J., Rengasamy, K.R.R., 2023. The potential role of extracellular vesicles in bioactive compound-based therapy: a review of recent developments. Crit. Rev. Food Sci. Nutr. 63, 10959–10973. ⟨https://www.tandfonline.com/doi/abs/10.1080/10408398.2022.2081667⟩.

Lu, X., Wang, C., Zhao, M., Wu, J., Niu, Z., Zhang, X., Simal-Gandara, J., Süntar, I., Jafari, S.M., Qiao, X., 2022. Improving the bioavailability and bioactivity of garlic bioactive compounds via nanotechnology. Crit. Rev. Food Sci. Nutr. 62, 8467–8496.

Mandhadi, J.R., Panneerselvam, T., Parasuraman, P., 2020. DESIGN, in silico modeling, toxicity study and synthesis of novel substituted semicarbazide derivatives of pyrimidine: an antitubercular agent. Curr. Bioact. Compd. 16, 294–301. ⟨https://www.ingentaconnect.com/content/ben/cbc/2020/00000016/00000003/art00010⟩.

Murugesan, S., 2022. and validation of bioactive compounds from Cynodon dactylon as potential neuroprotective agents against α-synuclein. Graph Theor. Netw. Anal. silico Explor. ⟨https://pmc.ncbi.nlm.nih.gov/articles/PMC9809135/⟩.

Naiknaware, R., Ajudia, R., Vekariya, H., Bansode, T., Rashinkar, G., Bansode, P., 2025. Ionic liquid [FcMeBIMIoct] [Br−] catalyzed multicomponent synthesis, anticancer activity, in silico ADMET, DFT, QSAR and molecular docking studies of new dihydropyrimidine-thiones. J. Mol. Liq. 426, 127313. https://doi.org/10.1016/j.molliq.2025.127313.

Palanichamy, C., Pavadai, P., Panneerselvam, T., Arunachalam, S., Babkiewicz, E., Ram Kumar Pandian, S., Shanmugampillai Jeyarajaguru, K., Nayak Ammunje, D., Kannan, S., Chandrasekaran, J., 2022. Aphrodisiac performance of bioactive compounds from Mimosa pudica Linn.: In silico molecular docking and dynamics simulation approach. Molecules 27, 3799. ⟨https://www.mdpi.com/1420-3049/27/12/3799⟩.

Panneerselvam, T., Kunjiappan, S., Govindaraj, S., Gopal, M., Natarajan, K., Hegde, Y.M., Shanmugam, N., Srinivas, G., Ravi, K., Natarajan, V., 2022. Graph Theoretical analysis, in silico modeling and molecular dynamic studies of (5-((2-chloropyridin-4-yl) oxy)-3-phenyl-1H-pyrazol-1-yl)-2-(4-substituted phenyl)-N, N-dimethylethen-1-amine derivatives for the treatment of breast cancer. Anticancer Agents Med. Chem. ⟨https://www.tandfonline.com/doi/abs/10.1080/10408398.2021.1929058⟩.

Patagar, D.N., Kusanur, R., Batakurki, S.R., Patra, S.M., Patil, N.R., Patil, J.H., 2023. 8-benzimidazolyl coumarin-3-oxadiazoles – Synthesis, docking studies and Anti-proliferative evaluation against breast cancer. J. Mol. Struct. 1294, 136377. https://doi.org/10.1016/j.molstruc.2023.136377.

Patil, P., Nerlekar, N., Rathod, S., Mhaldar, P., Najm, T., Bansode, P., Jadhav, J., Dandge, P., Choudhari, P., Pore, D., Rashinkar, G., 2024b. Novel sulphonamide-azaheterocycle conjugates and their anti-cancer, anti-inflammatory, anti-diabetic, anti-angiogenesis activity and molecular docking studies. Results Chem. 7, 101476. https://doi.org/10.1016/j.rechem.2024.101476.

Patil, P., Patil, P., Dandge, P., Bansode, P., Kumbhar, B., Chandane, W., Rathod, S., Choudhari, P., Khot, S., Valekar, N., Pore, D., Rashinkar, G., 2024a. Benzylpyrazolyl naphthoquinones as potential VEGFR-2, GPCR and PPAR inhibitors: Synthesis, anti-cancer evaluation, molecular docking and DFT studies. J. Mol. Struct. 1301, 137202. https://doi.org/10.1016/j.molstruc.2023.137202.

Ramesh, S., Almeida, S.D., Hammigi, S., Radhakrishna, G.K., Sireesha, G., Panneerselvam, T., Vellingiri, S., Kunjiappan, S., Ammunje, D.N., Pavadai, P., 2023. A review of PARP-1 inhibitors: assessing emerging prospects and tailoring therapeutic strategies. Drug Res. 73, 491–505. ⟨https://api.semanticscholar.org/CorpusID:264518281⟩.

Senthamarai Pandi, J., Pavadai, P., Sundar, L.M., Sankaranarayanan, M., Panneerselvam, T., Pandian, S.R.K., Kunjiappan, S., 2025. Pharmacokinetics and

brain tumor delivery studies of thymoquinone-encapsulated eudragit L100-coated solid-lipid nanoparticles. J. Clust. Sci. 36, 26. ⟨https://link.springer.com/article/10.1007/s10876-024-02751-5⟩.

Sumalatha, K., Theivendren, P., Rathinasamy, G., 2025. Solid lipid nanoparticle encapsulated beta-carotene for targeted breast cancer therapy: network pharmacology, molecular docking, and in vitro evaluation. Silico Res. Biomed., 100054. ⟨https://www.sciencedirect.com/science/article/pii/S3050787125000538⟩.

Theivendren, P., Kunjiappan, S., Pavadai, P., Shanmugam, A., Karunanithi, K., Gopal, M., Kiruthiga, N., 2025. Success stories: impactful applications of cancer biomarkers. in: The Potential of Cancer Biomarkers. Elsevier, pp. 297–331. ⟨https://www.sciencedirect.com/science/chapter/edited-volume/abs/pii/B9780443292798000156⟩.

Yan, Z., Chen, S., Igbokwe, C.J., Duan, Y., Hu, K., Cai, M., Zhang, H., 2025. Study on the interventional effect and molecular mechanism of HSP72 in regulating oxidative stress by watermelon seed peptide RDPEER. Food Chem. 478, 143748. ⟨https://www.sciencedirect.com/science/article/abs/pii/S0308814625009999⟩.

Yang, W., Cao, L., Lu, H., Huang, Y., Yang, W., Cai, Y., Li, S., Li, S., Zhao, J., Xu, W., 2024. Custom-printed microfluidic chips using simultaneous ratiometric fluorescence with "Green" carbon dots for detection of multiple antibiotic residues in pork and water samples. J. Food Sci. 89, 5980–5992. ⟨https://ift.onlinelibrary.wiley.com/doi/abs/10.1111/1750-3841.17239⟩.

Zabaleta, M.E., Forbes-Hernández, T.Y., Simal-Gandara, J., Quiles, J.L., Cianciosi, D., Bullon, B., Giampieri, F., Battino, M., 2020. Effect of polyphenols on HER2-positive breast cancer and related miRNAs: Epigenomic regulation. Food Res. Int. 137, 109623. ⟨https://www.sciencedirect.com/science/article/abs/pii/S0963996920306487⟩.

Zhang, J., Hassane Hamadou, A., Chen, C., Xu, B., 2023. Encapsulation of phenolic compounds within food-grade carriers and delivery systems by pH-driven method: A systematic review. Crit. Rev. Food Sci. Nutr. 63, 4153–4174. ⟨https://www.tandfonline.com/doi/abs/10.1080/10408398.2021.1998761⟩.

Zhou, C., Li, C., Siva, S., Cui, H., Lin, L., 2021. Chemical composition, antibacterial activity and study of the interaction mechanisms of the main compounds present in the Alpinia galanga rhizomes essential oil. Ind. Crops Prod. 165, 113441. ⟨https://www.sciencedirect.com/science/article/abs/pii/S0926669021002053⟩.

Zhu, Y., Gu, Z., Liao, Y., Li, S., Xue, Y., Firempong, M.A., Xu, Y., Yu, J., Smyth, H.D.C., Xu, X., 2022. Improved intestinal absorption and oral bioavailability of astaxanthin using poly (ethylene glycol)-graft-chitosan nanoparticles: preparation, in vitro evaluation, and pharmacokinetics in rats. J. Sci. Food Agric. 102, 1002–1011. ⟨https://scijournals.onlinelibrary.wiley.com/doi/abs/10.1002/jsfa.11435⟩.